2013 IEEE International Conference on Robotics and Automation (ICRA)
Karlsruhe, Germany, May 6-10, 2013

Real-Time Three-Dimensional Flexible Needle Tracking using Two-Dimensional Ultrasound

Gustaaf J. Vrooijink, Momen Abayazid and Sarthak Misra
University of Twente, The Netherlands

Abstract— **Needle insertion is one of the most commonly performed minimally invasive procedures. Visualization of the needle during insertion is key for either successful diagnosis or therapy. This work presents the real-time three-dimensional tracking of flexible needles during insertion into a soft-tissue simulant using a two-dimensional (2D) ultrasound transducer. The transducer is placed perpendicular to the needle tip to measure its position. During insertion the transducer is robotically repositioned to track the needle tip. Positioning of the transducer is accomplished by a compensator, that uses the needle insertion velocity corrected by needle tip velocities to determine out-of-plane motion. Experiments are performed to validate the needle tip pose during tracking. The maximum mean errors in needle tip position along the x-, y- and z-axes are 0.64 mm, 0.25 mm and 0.27 mm, respectively. The error in tip orientations (θ-about the y-axis and ϕ-about the z-axis) are 2.68° and 2.83°, respectively. This study demonstrates the ability to compute the needle tip pose using a 2D ultrasound transducer. The tip pose can be used to robotically steer needles, and thereby improve accuracy of medical procedures.**

I. INTRODUCTION

In numerous minimally invasive medical procedures, needles are inserted into tissue for diagnosis and therapy. The success of the procedure depends on needle placement accuracy. Needle misplacement can cause misdiagnosis (e.g., biopsies) and delayed or unsuccessful treatment (e.g., brachytherapy) [1], [2]. Needle insertion is often performed under image-guidance, e.g., computed tomography (CT) scans, fluoroscopy, magnetic resonance (MR) or ultrasound images. Using CT has drawbacks, as the patient is exposed to high doses of ionizing radiation during the procedure [3]. MR-guided procedures can only be combined with instruments made of nonmagnetic and dielectric materials [4]. Ultrasound is considered a safe and easily accessible imaging modality to visualize both the needle and target (lesion) during the procedure [5], [6]. For example, the smallest detectable size of a cancerous lesion in the breast is 2 mm [7].

During a procedure, rigid needles give the clinician limited steering capabilities to compensate for target motion, and initial misalignment between the needle and target. Recent studies show methods to deal with the mentioned problems, which involve pre-operative planning, target motion compensation and robot-controlled insertions [8]–[11]. Flexible needles with asymmetric (e.g., bevel) tips can be steered to compensate for target motion and initial misalignment.

The authors are affiliated with MIRA – Institute for Biomedical Technology and Technical Medicine. This research is supported by funds from the Netherlands Organization for Scientific Research (NWO). {g.j.vrooijink, m.abayazid, s.misra}@utwente.nl

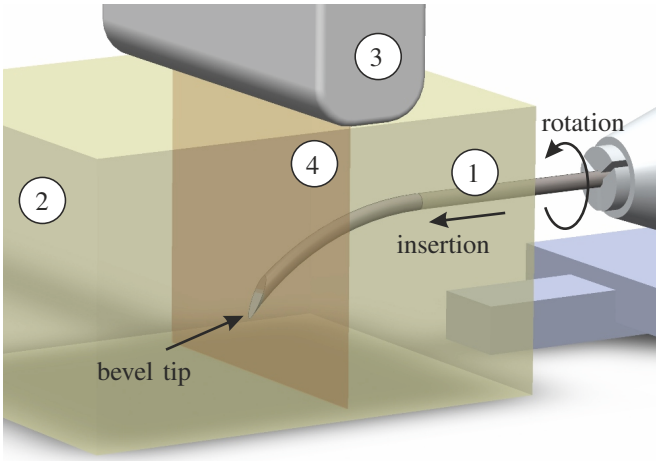

Fig. 1. A flexible needle ① with a bevel tip is inserted in the soft-tissue simulant ②. Depending on the orientation of the bevel tip, the needle can deflect in the three-dimensional space. The needle tip is tracked by an ultrasound transducer ③, which is placed perpendicular to the needle insertion direction. The two-dimensional ultrasound image plane ④ provides a radial cross-sectional view of the needle. During insertion the ultrasound transducer is robotically repositioned to track the needle tip in real-time.

Further, this enables the capability to avoid sensitive organs (e.g., blood vessels) and obstacles (e.g., bones). For all these capabilities the needle needs to be accurately controlled. Robotic needle insertion devices have been used in previous studies to improve the needle placement accuracy [11]–[16]. Some of these studies use two-dimensional (2D) ultrasound to assist the robotically inserted needles, but movement is limited to the 2D image plane [11], [13]. Neshat and Patel used real-time 2D ultrasound images to construct a volume in which curved needles are tracked [17]. However, the volume remains a compromise between its size and acquisition time. Tracking surgical instruments such as cardiac catheters using three-dimensional (3D) ultrasound images has also been demonstrated [18], [19]. However, the 3-8 mm diameter of these cardiac catheters (some equipped with markers) are significantly larger than the diameter (0.5-1.0 mm) of flexible needles. Therefore, the cardiac catheters will result in a more detailed reproduction than a flexible needle. Modern 3D ultrasound transducers available for real-time applications have a limited voxel resolution. Low voxel resolutions of 3D ultrasound limits accurate needle tip detection up to 3 mm [20]. Nadeau and Krupa described 3D target motion tracking with 2D ultrasound [21], but the allowed target motion was limited. No available studies to date describe real-time 3D tracking of flexible needles inserted into soft-tissue. This paper presents a novel technique to track flexible

978-1-4673-5642-8/13/$31.00 ©2013 IEEE

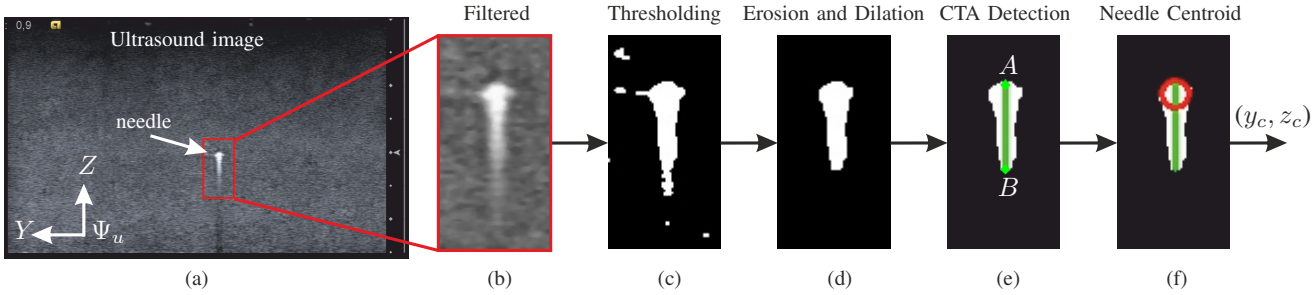

Fig. 2. Image processing methodology to determine the needle centroid location (y_c,z_c) in the ultrasound images. (a) The ultrasound input image is a radial cross-sectional view of the needle with the comet tail artifact (CTA). (b) In order to minimize speckle in the ultrasound image, a median filter is applied to the needle with the CTA. (c) A binary image is obtained by thresholding. (d) The remaining speckle in the image is removed by erosion and dilation. (e) A line detection algorithm using Hough transform is applied to detect the needle with the CTA. This line is denoted $\overline{AB}$. (f) In $\overline{AB}$, A represents the needle surface. The needle centroid (y_c, z_c) is evaluated as the center of the red circle (since the diameter of the needle is known).

needles in 3D using a 2D ultrasound transducer. The 2D ultrasound transducer is placed perpendicular to the needle insertion direction (Fig. 1). The transducer is unable to measure needle tip movement in its out-of-plane direction. Therefore, a compensator is used to evaluate the out-of-plane motion. The transducer is then repositioned by a positioning device to compensate for movement in the out-of-plane direction. This enables 3D real-time tracking of the needle tip through the soft-tissue simulant.

The paper is organized as follows: Section II describes the image processing algorithm used to detect the needle tip location using 2D ultrasound images. Further, the needle tip pose computations, and the image-guided motion controller to position the ultrasound transducer during insertion are discussed. Section III describes the setup and experiments performed to validate the performance of needle tip tracking method, and results are also presented. Finally in Section IV, we conclude and provide directions for future work.

II. METHODS

This section presents a method to track the needle tip in 3D by using a 2D ultrasound transducer. First, image processing to locate the needle in ultrasound images is described. Subsequently, computations required to determine the needle tip pose are explained. Finally, the controller which positions the transducer at the needle tip is presented.

A. Ultrasound Image Processing

Needle tip position feedback for control is provided by ultrasound image processing. The ultrasound transducer is placed perpendicular to the needle insertion direction (Fig. 1). The images show a 2D radial cross-sectional view of the needle, which has ideally a circular shape. However the circular shape is deformed by the reverberation artifact as shown in Fig. 2(a) [22]. Reverberation occurs when sound waves are repeatedly reflected between different boundaries, that are introduced by differences in acoustic impedances between materials. The acoustic impedance difference between needle and soft tissue is significant, which causes multiple and strong bouncing echoes in the needle. If the angle of reflection is almost perpendicular to the receivers in the transducer, the bouncing echoes return to the transducer. The resulting artifact which appears in images as a tail-shaped structure of equally spaced echoes along the ultrasound wave is often referred to as the comet tail artifact (CTA) [23]. The length of the tail-shaped structure depends on the echoes that are received by the transducer.

An image processing algorithm is developed to determine the location of the needle, which is affected by the CTA (Fig. 2). Ultrasound images with a radial cross-sectional view of the needle are used. The needle visibility is enhanced, and speckling is removed by applying basic image processing techniques such as, median filtering, thresholding, and erosion and dilation in Fig. 2(b), (c) and (d), respectively. A line detection algorithm based on Hough transform is used to find a set of vertical line segments describing the needle with the CTA. Each line segment must be at least the length of the needle diameter. We assume that the needle has a symmetric shape along the ultrasound wave (z-axis of frame (Ψ_u) in Fig. 2). By using both the symmetry property and the set of vertical line segments, a mean line segment ($\overline{AB}$) describing the needle with the CTA is determined (Fig. 2(e)). Changes in the length of the tail-shaped structure of the CTA will affect the mean line segment at B. The mean line segment at A represents a point on the surface of the needle. The needle centroid (y_c, z_c) is located on $\overline{AB}$, at a distance equal to the radius of the needle from A (Fig. 2(f)). If the transducer is properly positioned at the needle tip, the centroid (y_c, z_c) can be used to compute the needle tip pose.

B. Needle Tip Pose Computation

An overview of the various coordinate systems required to compute the needle tip pose are provided in Fig. 3. The needle is inserted with velocity ($\mathbf{v}_i$) along the x-axis of frame (Ψ_0) in the soft-tissue simulant by the needle insertion device (NID). In order to provide feedback, the needle tip position ($\mathbf{p}_t^0$) expressed in the fixed reference frame (Ψ_0),

$$\mathbf{p}_t^0 = \begin{bmatrix} p_x & p_y & p_z \end{bmatrix}^T, \tag{1}$$

must be computed. Positioning the ultrasound transducer at the needle tip allows the tip frame to be expressed in fixed reference frame by a series of coordinate transformations. Whereby the needle centroid (y_c, z_c), obtained by image processing, describes the needle tip frame with respect to ultrasound image frame. For computational simplicity, we

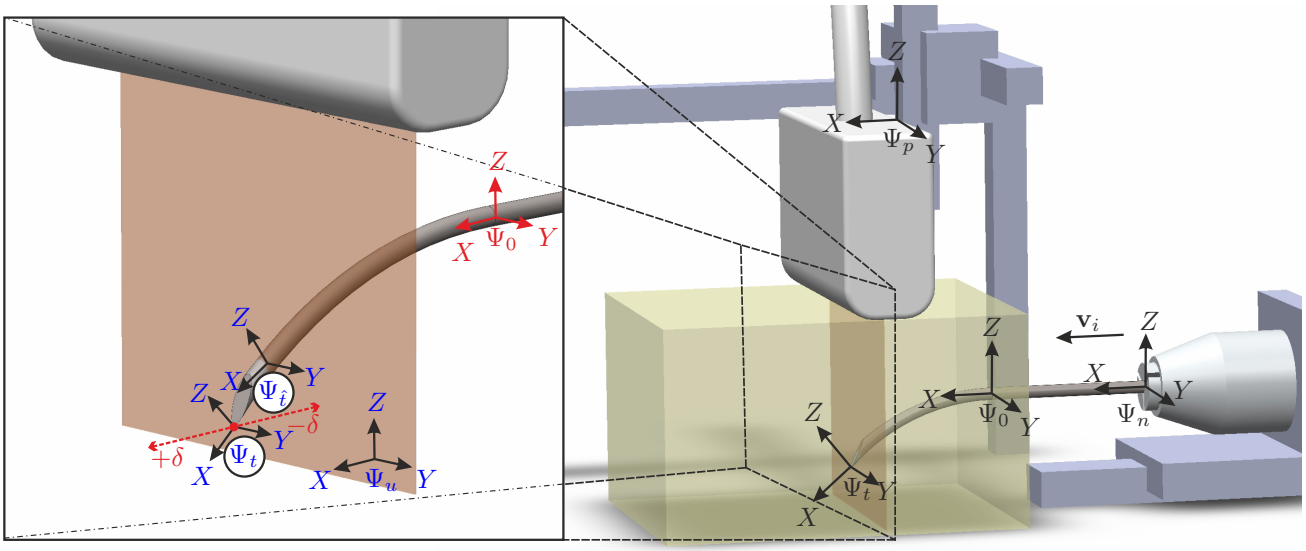

Fig. 3. Overview of the various coordinate systems required to compute the needle tip pose. Frame (Ψ_n) is located at the end-effector of the needle insertion device. Fixed reference frame (Ψ_0) is at the point where the needle enters the soft-tissue simulant, while frame (Ψ_t) is fixed to the needle tip. Frame (Ψ_p) is located at the end-effector of the positioning device, while frame (Ψ_u) is assigned to the two-dimensional ultrasound image. Frame ($\Psi_{\hat{t}}$) is at the needle tip as determined by the controller. The aberration in the transducer position along the needle insertion direction is denoted by $\pm\delta$.

assume frames (Ψ_u and Ψ_p) to coincide. The end-effector frame of the positioning device can be expressed in the fixed reference frame by position feedback. The consecutive transformations are used to compute the needle tip position ($\mathbf{p}_t^0$). In order to compute ($\mathbf{p}_t^0$) during needle insertion, repositioning of the transducer to compensate for out-of-plane motion (along the x-axis of frame (Ψ_0)) is required. We assume that the needle does not buckle during insertion. Thus, the needle tip velocity ($\|\dot{\mathbf{p}}_t^0\|$) equals to the insertion velocity ($\|\mathbf{v}_i\|$),

$$\|\mathbf{v}_i\| = \sqrt{\dot{p}_x^2 + \dot{p}_y^2 + \dot{p}_z^2}. \tag{2}$$

Hence, the needle tip velocity along the x-axis (frame (Ψ_0)) which must be compensated for is given by,

$$\dot{p}_x = \sqrt{\|\mathbf{v}_i\|^2 - \dot{p}_y^2 - \dot{p}_z^2}, \tag{3}$$

where $\dot{p}_y$ and $\dot{p}_z$ are the needle tip deflection velocities calculated by taking time derivatives of needle tip positions (p_y and p_z), respectively. The complete needle tip pose requires orientations (ψ, θ and ϕ) of the needle tip about the x-, y- and z-axes, respectively. Needle tip orientation can not be obtained by direct measurement. Although, the needle tip rotation about the y- and z-axes can be computed by,

$$\theta = \tan^{-1}\left(\frac{\Delta p_z}{\Delta p_x}\right) \text{ and } \phi = \tan^{-1}\left(\frac{\Delta p_y}{\Delta p_x}\right), \tag{4}$$

respectively, where Δp_x, Δp_y and Δp_z are small displacements in x-, y- and z-axes (frame (Ψ_0)), respectively. Needle tip orientation about the x-axis (ψ) is obtained from the NID, where we assumed no torsion along the needle shaft during rotation. Orientations (ψ, θ and ϕ) of the needle tip are used to determine rotation matrix $\mathbf{R}_t^0$. Thus, if the pose is known, the homogeneous transformation ($\mathbf{H}_t^0$) can be computed,

$$\mathbf{H}_t^0 = \begin{bmatrix} \mathbf{R}_t^0 & \mathbf{p}_t^0 \\ \mathbf{0}_3^T & 1 \end{bmatrix}, \tag{5}$$

that relates the needle tip frame (Ψ_t) to fixed reference frame (Ψ_0). It is essential to control the transducer position to accurately compute the needle tip pose during insertion.

C. Ultrasound Image-Guided Controller

The controller is used to position the ultrasound transducer, and to compute position feedback of the needle tip (Fig. 4). The needle tip position is denoted by $\mathbf{p}$, while the velocity ($\dot{\mathbf{p}}$) is calculated by taking the time derivative. For notational simplicity, we do not include frame Ψ_0 in the variables presented in this sub-section. The compensator is used to move the transducer according the needle tip velocity ($\dot{p}_x$). An estimation error in $\dot{p}_x$ results in a positioning error of the transducer along the x-axis (frame (Ψ_0)),

$$\delta = \mid p_x - \hat{p}_x \mid, \tag{6}$$

where $\hat{p}_x$ is the needle tip position along the x-axis (frame (Ψ_0)) as determined by the controller and δ is the absolute error in transducer position along the x-axis (frame (Ψ_0)), which is considered to be the transducer aberration. A needle tip pose error (between frames (Ψ_t and $\Psi_{\hat{t}}$)) in the computed needle tip pose is introduced by δ (Fig. 3). Therefore, the computed needle tip pose is denoted by $\mathbf{H}_{\hat{t}}^0$. By applying closed-loop control, the transducer aberration (δ) can be reduced, which also reduces the needle tip pose error. From ultrasound images it can be determined whether the needle is in- or out-of-plane. In the latter case, the transducer is positioned ahead of the needle. Thus, by scheduling of the velocity gain (K_e), the velocity required to move the transducer along the x-axis (frame (Ψ_0)) can be controlled in closed-loop. The gain K_e is used to increase or decrease the transducer velocity when the needle is in- or out-of-plane, respectively. Gain scheduling is chosen as,

$$K_e = \begin{cases} 1.05 & \text{if needle is in-plane} \\ 0.5 & \text{if needle is out-of-plane} \end{cases} \tag{7}$$

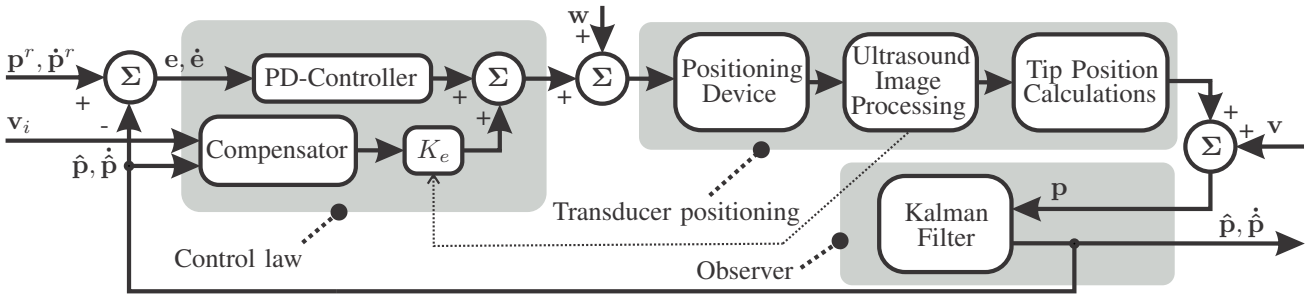

Fig. 4. The controller architecture used to track the needle tip in real-time, as it is inserted through the soft-tissue simulant. Ultrasound transducer positioning along the x-axis (frame (Ψ_0)) is performed by a compensator and gain scheduler (K_e) according (3) and (7), respectively. The proportional-derivative-(PD)-controller (proportional gain ($K_p = 0.4$) and derivative gain ($K_d = 0.1$)) is used to compensate for needle tip motion along the y-axis (frame (Ψ_0)), while motion in z-axis (frame (Ψ_0)) is not compensated for. A Cartesian robotic system is used to position the transducer at the needle tip, in order to measure its position, which is denoted by $\mathbf{p}$. The time derivative of $\mathbf{p}$, which represents the needle tip velocity is given by $\dot{\mathbf{p}}$. The reference positions and velocities are denoted by $\mathbf{p}^r$ and $\dot{\mathbf{p}}^r$, respectively. The tracker position and velocity errors are denoted by $\mathbf{e}$ and $\dot{\mathbf{e}}$, respectively. The Kalman observer is used to minimize the effects of process ($\mathbf{w}$) and measurement ($\mathbf{v}$) noise on the states ($\mathbf{p}$ and $\dot{\mathbf{p}}$), and to predict the subsequent states. The needle tip position and velocity obtained from the state observer are denoted $\hat{\mathbf{p}}$ and $\dot{\hat{\mathbf{p}}}$, respectively.

By employing a gain scheduling controller, the transducer is forced to move towards the needle tip and thus, minimizes δ. Hence, the needle tip pose ($\mathbf{H}_{\hat{t}}^0$) can be computed. Control of the transducer along the y-axis (frame (Ψ_0)) is done by a standard proportional-derivative-(PD)-controller, which allows tracking of the needle beyond the width (5.5 cm) of the ultrasound transducer image plane. The z-axis (frame (Ψ_0)) is not controlled during needle tracking, but is used to position the transducer at the surface of the soft-tissue simulant. A Kalman observer is added to minimize the influence of noise on the states ($\mathbf{p}$ and $\dot{\mathbf{p}}$), and to predict the subsequent states using the needle tip velocity [24]. If the transducer is placed ahead of the needle, the subsequent states are based on constant needle tip velocity. Without measurement updates the uncertainty of the projected states increase, which makes it important to minimize the duration of measurement absence. The Kalman gain will be adjusted according the increased uncertainty of the predicted states when measurement is available, which ensures a quick decrease in estimation error.

III. Experiments and Validation

This section describes the experimental setup used to track a needle inserted through the soft-tissue simulant. Two types of experiments are performed to evaluate the performance of the needle tip tracking system, and results are presented.

A. Experimental Setup

The experimental setup used to track flexible needles during insertion is shown in Fig. 5. The used needles are fabricated from Nitinol (nickel and titanium alloy, with a Young's Modulus of 75 GPa), which are bevel-tipped with an angle of 30°. Two different needle diameters are used, ϕ 0.5 mm and ϕ 1.0 mm. A gelatin mixture is used to simulate breast-tissue elasticity properties [25]. The elasticity properties of 35 kPa (Young's Modulus) are obtained by mixing (by-weight) gelatin powder (14.9%) (Dr. Oetker, Ede, The Netherlands) with water (84.1%) and silica gel 63 (1.0%) (E. Merck, Darmstadt, Germany) [26]. Silica gel is added to mimic the acoustic scattering effects of tissue, that are visible in ultrasound images. The needle is inserted by the two-DOF NID. The NID allows the needle to be translated along and rotated about the longitudinal axis [27]. The ultrasound images are obtained by an 18 MHz transducer using a Siemens Acuson S2000 ultrasound system (Siemens AG, Erlangen, Germany). Ultrasound transmission gel is used to improve the transmission of acoustic waves between transducer and soft-tissue simulant. During image acquisition the following settings were used: A frequency of 16 MHz, −12 dB power level and 3 cm scan depth. The images are transferred for image processing to a computer (64-bit, 2.27 GHz Intel Xeon, 12-GB internal memory, 64-bit Windows 7) via S-video output at 25 Hz. The resolution corresponding to the scan depth (3 cm) is 0.12 mm per pixel. The ultrasound transducer is clamped in a three-DOF Cartesian positioning device. The device consists of three orthogonally-placed translational stages LX30, LX26 and LX20 (Misumi Group Inc., Tokyo, Japan) to enable movement in x-, y- and z-axes (frame (Ψ_p)) in Fig. 3, respectively. Each stage is actuated by an ECMax22 motor with a GP32/22 gearhead (Maxon Motor, Sachseln, Switzerland), which is velocity controlled by an Elmo Whistle 2.5/60 motor controller (Elmo Motion Control Ltd, Petach-Tikva, Israel). The positioning accuracy of the device is determined at 27 μm, 35 μm and 41 μm along the x-, y- and z-axes (frame (Ψ_p)), respectively. The ultrasound transducer is securely clamped by a 3D-printed holder.

B. Experimental Plan

A reference measurement is used to validate the needle tip pose obtained using ultrasound tracking. The needle tip pose for an undeflected needle can also be computed by,

$$\mathbf{H}_t^0 = \mathbf{H}_n^0 \mathbf{H}_t^n, \tag{8}$$

where $\mathbf{H}_n^0$ is the homogeneous transformation from NID frame (Ψ_n) relative to frame (Ψ_0), and $\mathbf{H}_t^n$ is the transformation from needle tip frame (Ψ_t) relative to NID frame (Ψ_n) (Fig. 3). For an undeflected needle, the homogeneous transformation matrix ($\mathbf{H}_t^n$) can be described by a translation mapping in the x-axis (frame (Ψ_0)) equal to the length of the needle. If the needle is rotated during insertion with sufficiently high rotational velocity relative to

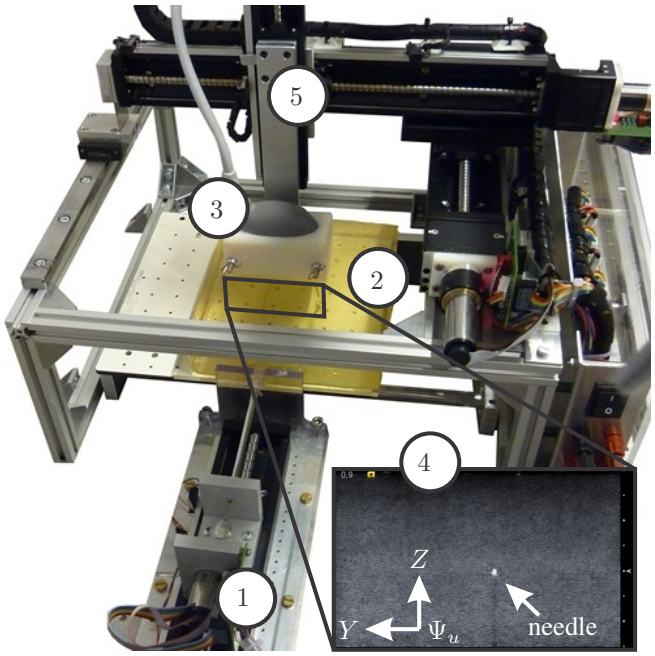

Fig. 5. The experimental setup used for three-dimensional needle tip tracking. ① Needle insertion device. ② Soft-tissue simulant based on a gelatin mixture. ③ Ultrasound transducer. ④ Ultrasound image with a radial cross-sectional view of the needle. ⑤ Robotic positioning device of the ultrasound transducer.

its insertion velocity, a straight insertion will be achieved i.e., drilling motion (Case I). For such a needle motion profile, the tip pose error between frames ((Ψ_t) and ($\Psi_{\hat{t}}$)) can be formulated by a closed kinematic chain,

$$\mathbf{E} = \mathbf{H}_n^t \mathbf{H}_0^n \mathbf{H}_{\hat{t}}^0, \tag{9}$$

where $\mathbf{E} \in \mathbb{R}^{4\times4}$ represents the needle tip pose error, which is ideally described by the identity matrix. The experiments performed to validate real-time needle tip tracking by evaluating the needle tip pose error ($\mathbf{E}$) are given in Case I (Table I). In Case II, the needle is tracked while it is inserted and rotated (360°) along the insertion length, which results in a helical needle insertion profile. After insertion, the transducer is swept with a velocity of 3 mm/s over the soft-tissue simulant surface to acquire the needle shape. We assume that the needle shape remains unchanged after insertion. The static needle shape data can be compared to real-time needle tip tracking data. For points along the x-axis (frame (Ψ_0)), the needle deflection along and about y- and z-axes (frame (Ψ_0)) are evaluated. The accuracy in needle tip deflection is validated by Case II (Table I).

C. Experimental Results

The results from experiments in Cases I and II are provided in Table II. Each experiment is repeated ten times. The mean absolute errors in the tracked tip positions (ϵ_x, ϵ_y and ϵ_z) and orientations (ϵ_θ and ϵ_ψ) during insertion between frames (Ψ_t and $\Psi_{\hat{t}}$) are reported. In Case I, a ϕ 1.0 mm needle is used to increase the likelihood of a straight insertion. For Case II, a ϕ 0.5 mm needle is used to increase deflection during insertion. Maximum errors in positions are 0.64 mm (Case I.3), 0.25 mm (Case II) and 0.27 mm (Case II) along the x-, y- and z-axes, respectively. Maximum errors in orientation about the y-axis (θ) and z-axis (ϕ) are 2.68° (Case I.4) and 2.83° (Case I.4), respectively.

TABLE I

EXPERIMENTAL CASES: CASE I-VALIDATION OF REAL-TIME NEEDLE TIP TRACKING. POSITIONS AND ORIENTATIONS OF THE NEEDLE TIP ARE EVALUATED BY THE NEEDLE TIP POSE ERROR ($\mathbf{E}$). TRACKING IS VALIDATED FOR THREE INSERTION VELOCITIES ($\|\mathbf{v}_i\|$) AND TWO INSERTION DEPTHS (d). A NEEDLE DIAMETER (ϕ) OF 1.0 MM IS USED. FOR EVERY MILLIMETER INSERTED, A FULL ROTATION (360°) IS PERFORMED. CASE II-VALIDATION OF NEEDLE TIP DEFLECTION DURING INSERTION. THE NEEDLE WITH A DIAMETER (ϕ) OF 0.5 MM IS INSERTED AND ROTATED (360°) ALONG THE INSERTION LENGTH (d) TO OBTAIN A HELICAL INSERTION PROFILE.

	$\|\mathbf{v}_i\|$ [mm/s]			d [mm]		
Case	1	3	5	40	80	110
I.1	√			√		
I.2		√		√		
I.3			√	√		
I.4	√				√	
I.5		√			√	
I.6			√		√	
II		√				√

D. Discussion

In Case I (drilling motion), frame (Ψ_t) is attached to the needle tip which rotates about its x-axis at high rotational velocity (full rotation each mm inserted). This results in a continuously interchanging y- and z-axes. Hence, we observe similar values for ϵ_y and ϵ_z. Experiments from Case I show that an increase in needle insertion velocity increases the error (ϵ_x), which could be explained by an increase in aberration of the ultrasound transducer during insertions at higher velocities. By decreasing the needle insertion velocity from 5 mm/s to 1 mm/s, the resulting error (ϵ_x) reduces by 62.5% (Case I.3 versus Case I.1) and 50.0% (Case I.6 versus Case I.4). Further from Case I, it can be observed that for longer insertions (80 mm), the maximum errors (ϵ_y and ϵ_z) both increase by 57.1%. Since different needle insertion velocities results in negligible differences in needle deflection errors (ϵ_y and ϵ_z) for Case I, Case II is only conducted at 3 mm/s insertion velocity. Although it can not be ruled out that tracking accuracy deteriorates over the insertion depth. In Case II, errors (ϵ_y and ϵ_z) increased by 13.6% and 22.7% as compared to Case I.6, respectively. This could be explained by the increased insertion depth.

IV. CONCLUSIONS AND FUTURE WORK

This study presents a 3D needle tip tracking system that uses 2D ultrasound images. A 2D ultrasound transducer is placed perpendicular to the needle tip to measure its position in real-time. During insertion a positioning device is used to reposition the ultrasound transducer, which provides needle tip pose feedback. In order to target the smallest detectable lesions of 2 mm, accurate feedback is required. Experiments show maximum errors in tip positions along the x-, y- and z-axes are 0.64 mm, 0.25 mm and 0.27 mm, respectively. Maximum error in tip orientations about y-(θ)- and z-(ϕ)-axes are observed as 2.68° and 2.83°, respectively.

TABLE II

NEEDLE POSITION AND ORIENTATION ERRORS FOR CASES I AND II ARE PRESENTED. MEAN ABSOLUTE ERRORS BETWEEN FRAMES (Ψ_t AND $\Psi_{\hat{t}}$) ARE REPORTED WITH THEIR STANDARD DEVIATIONS. ERRORS (ϵ_x, ϵ_y AND ϵ_z) REPRESENTS THE POSITION ERRORS ALONG THE x-, y- AND z-AXES, RESPECTIVELY, WHILE ϵ_θ AND ϵ_ϕ REPRESENT THE ORIENTATION ERRORS ABOUT THE y- AND z-AXES, RESPECTIVELY. *Please refer to the attached video that demonstrates the results of real-time three-dimensional tracking.*

Case	ϵ_x [mm]	ϵ_y [mm]	ϵ_z [mm]	ϵ_θ [degree]	ϵ_ϕ [degree]
I.1	0.24±0.16	0.14±0.04	0.14±0.04	2.57±0.47	2.59±0.47
I.2	0.36±0.10	0.11±0.04	0.11±0.04	1.58±0.32	1.57±0.34
I.3	0.64±0.11	0.13±0.08	0.13±0.10	1.68±0.65	1.69±0.78
I.4	0.24±0.10	0.18±0.08	0.18±0.08	2.68±1.22	2.83±1.36
I.5	0.31±0.01	0.15±0.06	0.15±0.06	1.13±1.32	1.40±1.43
I.6	0.48±0.09	0.22±0.12	0.22±0.12	1.14±0.29	1.19±0.32
II	-	0.25±0.06	0.27±0.06	1.63±0.57	1.39±0.24

For future work, we will combine tracking with needle steering updated by a path planner, which allows the needle to be steered around obstacles towards a target. By combining these systems, improved accuracy of minimally invasive medical procedures can be achieved. Also modifications to the transducer positioning device will be made to allow tracking over curved soft-tissue surfaces while ensuring that the transducer is in contact with tissue. This will be accomplished by coupling ultrasound images to data from a force sensor. Torsional stiffness and bucking of the flexible Nitinol needles will also be investigated. Biological tissue provides a more realistic testing scenario compared to gelatin-based soft-tissue simulant used in this study. Hence, needle tip tracking in biological tissue will be studied. Nonetheless, our proposed method demonstrates the feasibility to track needles suitable for clinical applications such as breast and prostate biopsies, and brachytherapy.

REFERENCES

[1] J. H. Youk, E.-K. Kim, M. J. Kim, J. Y. Lee, and K. K. Oh, "Missed breast cancers at us-guided core needle biopsy: How to reduce them," *Radiographics*, vol. 27, no. 1, pp. 79–94, 2007.

[2] S. Nag, W. Bice, K. DeWyngaert, B. Prestidge, R. Stock, and Y. Yu, "The american brachytherapy society recommendations for permanent prostate brachytherapy postimplant dosimetric analysis," *International Journal of Radiation Oncology Biology Physics*, vol. 46, no. 1, pp. 221–230, 2000.

[3] H. Fred, "Drawbacks and limitations of computed tomography: views from a medical educator," *Texas Heart Institute Journal*, vol. 31, no. 4, pp. 345–348, 2004.

[4] G. Fischer, I. Iordachita, C. Csoma, J. Tokuda, S. DiMaio, C. Tempany, N. Hata, and G. Fichtinger, "Mri-compatible pneumatic robot for transperineal prostate needle placement," *IEEE/ASME Transactions on Mechatronics*, vol. 13, no. 3, pp. 295–305, 2008.

[5] S. G. Shulman and D. E. March, "Ultrasound-guided breast interventions: Accuracy of biopsy techniques and applications in patient management," *Seminars in Ultrasound, CT, and MRI*, vol. 27, no. 4, pp. 298–307, 2006.

[6] Y.-C. Wu, D.-R. Chen, and S.-J. Kuo, "Personal experience of ultrasound-guided 14-gauge core biopsy of breast tumor," *European Journal of Surgical Oncology (EJSO)*, vol. 32, no. 7, pp. 715–718, 2006.

[7] Stjoeshealth.org, "The importance of mammography." http://www.stjoeshealth.org/, 2011.

[8] N. Abolhassani, R. V. Patel, and M. Moallem, "Needle insertion into soft tissue: A survey," *Medical Engineering and Physics*, vol. 29, no. 4, pp. 413–431, 2007.

[9] J. op den Buijs, M. Abayazid, C. L. de Korte, and S. Misra, "Target motion predictions for pre-operative planning during needle-based interventions," in *Proceedings of the IEEE International Conference on Engineering in Medicine and Biology Society (EMBC)*, pp. 5380–5385, Boston, Massachusetts, USA, September 2011.

[10] M. Abayazid, J. op den Buijs, C. L. de Korte, and S. Misra, "Effect of skin thickness on target motion during needle insertion into soft-tissue phantoms," in *Proceedings of the IEEE RAS/EMBS International Conference on Biomedical Robotics and Biomechatronics (BioRob)*, pp. 755–760, Rome, Italy, June 2012.

[11] J. Hong, T. Dohi, M. Hashizume, K. Konishi, and N. Hata, "An ultrasound-driven needle-insertion robot for percutaneous cholecystostomy," *Physics in Medicine and Biology*, vol. 49, no. 3, pp. 441–455, 2004.

[12] V. Kallem and N. Cowan, "Image guidance of flexible tip-steerable needles," *IEEE Transactions on Robotics*, vol. 25, no. 1, pp. 191–196, 2009.

[13] Z. Neubach and M. Shoham, "Ultrasound-guided robot for flexible needle steering," *IEEE Transactions on Biomedical Engineering*, vol. 57, no. 4, pp. 799–805, 2010.

[14] D. Glozman and M. Shoham, "Image-guided robotic flexible needle steering," *IEEE Transactions on Robotics*, vol. 23, no. 3, pp. 459–467, 2007.

[15] R. Webster III, J. Memisevic, and A. Okamura, "Design considerations for robotic needle steering," in *Proceedings of the IEEE International Conference on Robotics and Automation (ICRA)*, pp. 3588–3594, Barcelona, Spain, April 2005.

[16] J. A. Engh, G. Podnar, S. Y. Khoo, and C. N. Riviere, "Flexible needle steering system for percutaneous access to deep zones of the brain," in *Proceedings of the IEEE Annual Northeast Bioengineering Conference (NEBEC)*, pp. 103–104, Easton, Pennsylvania, USA, April 2006.

[17] H. Neshat and R. Patel, "Real-time parametric curved needle segmentation in 3d ultrasound images," in *Proceedings of the IEEE RAS EMBS International Conference on Biomedical Robotics and Biomechatronics (BioRob)*, pp. 670–675, Scottsdale, USA, October 2008.

[18] P. M. Novotny, J. A. Stoll, N. V. Vasilyev, P. J. del Nido, P. E. Dupont, T. E. Zickler, and R. D. Howe, "Gpu based real-time instrument tracking with three-dimensional ultrasound," *Medical Image Analysis*, vol. 11, no. 5, pp. 458–464, 2007.

[19] J. Stoll, H. Ren, and P. Dupont, "Passive markers for tracking surgical instruments in real-time 3d ultrasound imaging," *IEEE Transactions on Medical Imaging*, vol. 31, no. 3, pp. 563–575, 2012.

[20] M. Aboofazeli, P. Abolmaesumi, P. Mousavi, and G. Fichtinger, "A new scheme for curved needle segmentation in three-dimensional ultrasound images," in *Proceedings of the IEEE International Symposium on Biomedical Imaging: From Nano to Macro (ISBI)*, pp. 1067–1070, Piscataway, USA, July 2009.

[21] C. Nadeau and A. Krupa, "Intensity-based direct visual servoing of an ultrasound probe," in *Proceedings of the IEEE International Conference on Robotics and Automation (ICRA)*, pp. 5677–5682, Shanghai, China, May 2011.

[22] J. E. Aldrich, "Basic physics of ultrasound imaging," *Critical Care Medicine*, vol. 35, no. 5, pp. S131–S137, 2007.

[23] J. Huang, J. Triedman, N. Vasilyev, Y. Suematsu, R. Cleveland, and P. Dupont, "Imaging artifacts of medical instruments in ultrasound-guided interventions," *Journal of Ultrasound in Medicine*, vol. 26, no. 10, pp. 1303–1322, 2007.

[24] Y. Bar-Shalom, X. R. Li, and T. Kirubarajan, *Estimation with Applications to Tracking and Navigation*. New York, USA: John Wiley & Sons., 2001.

[25] A. Gefen and B. Dilmoney, "Mechanics of the normal woman's breast," *Technology and Health Care*, vol. 15, no. 4, pp. 259–271, 2007.

[26] R. J. Roesthuis, M. Abayazid, and S. Misra, "Mechanics-based model for predicting in-plane needle deflection with multiple bends," in *Proceedings of the IEEE International Conference on Biomedical Robotics and Biomechatronics (BioRob)*, pp. 69–74, Rome, Italy, June 2012.

[27] R. J. Roesthuis, Y. R. J. van Veen, A. Jayha, and S. Misra, "Mechanics of needle-tissue interaction," in *Proceedings of the IEEE International Conference on Intelligent Robots and Systems (IROS)*, pp. 2557–2563, San Francisco, California, USA, September 2011.